Properties of gallium oxide thin films grown by ion beam sputter deposition at room temperature

Dmitry Kalanov,[1, a)] Yeliz Unutulmazsoy,[1] Daniel Spemann,[1] Jens Bauer,[1] André Anders,[1,2] and Carsten Bundesmann[1]

[1)]*Leibniz Institute of Surface Engineering (IOM), Permoserstraße 15, 04318 Leipzig, Germany*

[2)]*Felix Bloch Institute of Solid State Physics, Leipzig University, Linnéstraße 5, 04103 Leipzig, Germany*

Gallium oxide thin films were grown by ion beam sputter deposition (IBSD) at room temperature on Si substrates in dependence on various process parameters: primary ion energy, primary ion species (O_2^+ and Ar^+), sputtering geometry (ion incidence angle α, polar emission angle β), and O_2 background pressure. No substrate heating was applied, because the goal of these experiments was to investigate the impact of the energetic film-forming species on thin film properties. The films were characterized with regard to the film thickness, growth rate, crystallinity, surface roughness, mass density, elemental composition and its depth profiles, and optical properties. All films were found to be amorphous with a surface roughness of less than 1 nm. The stoichiometry of the films improved with an increase in the energy of film-forming species. The mass density and the optical properties, including the index of refraction, are correlated and show a dependency on the kinetic energy of the film-forming species. The ranges of IBSD parameters, which are most promising for further improvement of the film quality, are discussed.

---

a)Email: dmitry.kalanov@iom-leipzig.de

I.   INTRODUCTION

Gallium oxide (Ga_2O_3) is an ultrawide-bandgap semiconductor, which is gaining increasing attention in recent years due to its promising material properties, such as large band gap energy and high breakdown field strength[1,2]. In particular, the most stable phase, monoclinic $\beta-Ga_2O_3$, has a band gap energy of about 4.9 eV, Ref.[3] and a breakdown field strength of up to 8 MV/cm, Ref.[4] These parameters enable the use of Ga_2O_3 in solar-blind UV detectors and gas sensors, as well as in ultra-high power electronics. The latter is crucial for the development of modern applications like photovoltaic inverters for wind power plants or high-power drives for transportation systems[5]. Amorphous gallium oxide thin films also have shown promising results as a transport layer in solar cells[6–9].

Typically, high-quality epitaxial Ga_2O_3 thin films are deposited by metal organic vapor-phase epitaxy (MOVPE)[10–12], plasma-assisted molecular beam epitaxy (PA-MBE)[13–19], or pulsed laser deposition (PLD)[3,20,21]. Amorphous and polycrystalline films have been also deposited using electron beam evaporation (EBE)[22,23], plasma-enhanced chemical vapor deposition (PECVD)[24], atomic layer deposition (ALD)[25,26] and radio frequency magnetron sputtering (RF-MS)[23,27–32].

Ion beam sputter deposition (ISBD) is a physical vapor deposition (PVD) technique known for superior opportunities for control over the properties of film-forming particles and, therefore, over the properties of the growing films[33]. IBSD involves the generation of energetic film-forming species with energies up to several hundred eV. Particle energies can be selectively adapted to provide intrinsic heating to the growing film, enhancing surface and bulk diffusion, while trying to minimize the formation of defects. On top of that, locations of primary ion generation, sputtering and thin film growth are separated in space, and the sputter geometry, ion energy, and ion species can be varied independently. Also, the substrate can be placed at different emission angles, which gives another degree of freedom. The spatial separation eliminates interaction between the ion source, the target, and the substrate, and it minimizes the number of undesired processes, such as arcing or arrival of particulates or droplets to the surface. Recently, IBSD with an Ar^+ ion beam was successfully used to deposit Ga_2O_3 films of high crystalline quality at substrate temperatures up to 650 °C[34]. It was shown, that the crystallinity of the films can be varied by selecting the substrate material, growth temperature, and oxygen partial pressure.

The present work is focused on the systematic investigation of properties of gallium oxide thin films, grown by IBSD, in dependence on various process parameters: sputtering geometry (ion incidence angle α, polar emission angle β), primary ion energies and ion species, as well as O_2 partial pressure. In the previous work, the properties of the film-forming species were studied for the same parameter sets through the measurements of energy distribution functions of secondary ions[35]. The main aim of the work is to correlate the properties of film-forming particles with the properties of deposited films by analyzing the energetic impact of those particles. For this reason, the films are deposited at room temperature, to separate the effects of substrate heating and intrinsic ion heating. In turn, it should help to identify the process parameter space, in which these energetic effects are beneficial for the film quality, and build a basis for the further optimization of the IBSD process for the growth of highly crystalline Ga_2O_3 films.

II. EXPERIMENT

A. Film deposition

The IBSD setup for film deposition is schematically shown in Figure 1. The setup consists of a broad-beam ion source, a target holder, and a substrate holder. The ion beam source and the target holder are placed on rotary tables with axes of rotation aligned with the center of the target surface. By rotating the ion source and the target, the ion incidence angle α can be set. The distances from the source to target and target to substrates are about 15 cm.

The in-house developed broad-beam ion source is based on inductively coupled radio-frequency (RF) plasma and is equipped with a three-grid multi-aperture extraction system with a diameter of 16 mm[36]. To minimize the grid erosion, Ti was selected as a grid material. O_2 or Ar were used as the process gases with volumetric flow rates of 7 sccm or 2.5 sccm, respectively. The ion source was operated with an RF-power of 130 W, and ion energies of $E_{ion} = 500$ eV, 1000 eV, or 1500 eV. Depending on the process parameters, the total ion beam current was between 7 mA and 14 mA. A current density profile had a Gaussian shape, with the divergence angle of about $3° - 5°$ for primary ions with energies of 1 keV - 1.5 keV, and up to $10°$ for ions with energies of 500 eV for 95% of the beam current[37–39]. The full
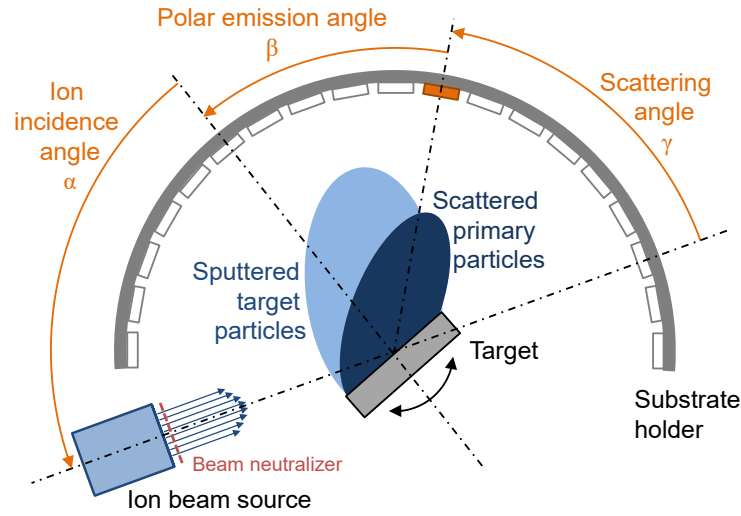
FIG. 1. Sketch of the experimental setup for ion beam sputter deposition.

widths at half maximum (FWHM) of the ion beam current profiles were about 50 mm for $E_{ion} < 1000$ eV, and around 30 mm for $E_{ion} = 1000$ eV[40]. The background process pressure was varied by introducing O_2 into the vacuum chamber. This additional oxygen flow was set to 5 sccm, 10 sccm, or 20 sccm. Combined with the flow through the ion source in case of O_2^+ ion beam, it resulted in 4 values of O_2 partial pressure being studied: 8.5×10^{-3} Pa, 1.7×10^{-2} Pa, 2.3×10^{-2} Pa, and 3.4×10^{-2} Pa. In case of Ar^+ ion beam, the O_2 partial pressures were 8×10^{-3} Pa, 1.5×10^{-2} Pa, and 2.7×10^{-2} Pa. The case of sputtering with Ar^+ ions without extra O_2 was also studied.

The substrate holder has a semi-circular shape with a possibility to place multiple substrates at polar emission angles in steps of 10°. Due to the size of the ion beam source, the minimum polar emission angle is given by $\beta = 20° - \alpha$. The maximum polar emission angle is $\beta = 80°$. It allowed us to mount up to 13 substrates for a single deposition (for $\alpha = 60°$). The sets of process parameters are summarized in Table I.

The thin films were grown on Si[100] (20×20) mm^2 substrates (CrysTec). The Ga_2O_3 target was ceramic, 4 inches in diameter, 6 mm thick, with purity of 99.99%, produced by powder sintering (Testbourne Ltd.). To prevent the accumulation of the positive charge on the target surface, a tungsten filament cathode neutralizer[41] was placed in front of the ion beam source. The total electron emission current was obtained by ruling out the effect

TABLE I. List of process parameter sets: E_{ion} is the primary ion energy, α and β are the angle of incidence and polar emission angle, respectively, t is the deposition time, and d_{max} is the maximum film thickness in the set.

Ion species	E_{ion} (eV)	α (°)	β (°)[a]	O_2 pressure (Pa)	t (min)	d_{max} (nm)
O_2	500	30	-10 to 80 (10)	$8.5 \cdot 10^{-3}$	420	76
O_2	1500	30	-10 to 80 (10)	$8.5 \cdot 10^{-3}$	300	123
O_2	1000	30, 60	-40 to 80 (10)	$8.5 \cdot 10^{-3}$	300	98, 151
O_2	1000	30	-10 to 80 (10)	$8.5 \cdot 10^{-3}, 1.7 \cdot 10^{-2},$ $2.3 \cdot 10^{-2}, 3.4 \cdot 10^{-2}$	300	98, 105, 101, 100
Ar	1000	30	-10 to 80 (10)	no O_2, $8.0 \cdot 10^{-3}$, $1.5 \cdot 10^{-2}, 2.7 \cdot 10^{-2}$	105	96, 96, 88, 83

[a] Minimum to maximum (increment).

of the charge accumulation on the energy distributions of sputtered ions[35]. Without beam neutralization, the distributions were significantly affected by the charge, accumulated on the target surface. The emission current was increased until the energy distributions stopped changing. The final current was fixed at 120 mA, slightly above the threshold value. Since only a portion of the emitted electrons is attracted by the space charge of the ion beam, a higher current value is necessary to compensate the charge on the target completely.

B. Film characterization

The gallium oxide films were characterized for the film thickness, growth rates, crystallinity, surface roughness, mass density, chemical composition, and optical properties.

Film thickness d and optical properties were determined using spectroscopic ellipsometry. The growth rate was obtained by dividing the thickness d by deposition time t. The spectra of ellipsometric parameters were recorded in a wavelength range from $\lambda = 193$ nm to $\lambda = 1700$ nm (corresponding to the photon energies from $E_p \approx 6.4$ eV to $E_p \approx 0.7$ eV) at four angles of incidence (60°, 65°, 70°, 75°) using a dual-rotating-compensator type ellipsometer RC2-DI (J. A. Woollam Co., Inc.).

The ellipsometric data were analyzed under the assumption of a 3-layer optical model: Si substrate - native SiO_2 layer - deposited gallium oxide layer. For the optical parameters of the Si substrate and the native SiO_2 layer, the tabulated values from literature were used[42]. For modeling of the optical properties of the gallium oxide layer, the following complex model dielectric function (MDF, dependent on the photon energy E_p) was used for fitting the measured data:

$$\widetilde{\varepsilon}(E_p) = \varepsilon_1(E_p) + i \cdot \varepsilon_2(E_p) = \varepsilon_\infty + \widetilde{\varepsilon}_{TL}(E_p) \tag{1}$$

Here ε_∞ is a high-frequency dielectric constant, which accounts for all electronic contributions outside the experimental photon energy range, and $\widetilde{\varepsilon}_{TL}(E_p)$ is a Tauc-Lorentz (TL) term. TL model is widely used for modeling the optical properties of amorphous or polycrystalline semiconductors or dielectrics in the spectral region of interband transitions[43–45] and, in particular, for Ga_2O_3[25,26,46,47] or its alloys[48,49].

The Tauc-Lorentz term is a combination of a classical Lorentz oscillator with a Tauc joint density of states. In this work, one TL term was used. The imaginary part of the term dependent on the photon energy E_p reads

$$\varepsilon_{2,TL}(E_p) = \begin{cases} \dfrac{A_{TL}B_{TL}E_{0,TL}(E_p - E_{g,TL})^2}{(E_p^2 - E_{0,TL}^2)^2 + B_{TL}^2 E_p^2} \cdot \dfrac{1}{E_p}, & E_p > E_g, \\ 0, & E_p \le E_g, \end{cases} \tag{2}$$

where A_{TL}, B_{TL}, and $E_{0,TL}$ are amplitude, broadening term, and peak transition energy, respectively. $E_{g,TL}$ is the Tauc band gap energy. The real part of the term, $\varepsilon_{1,TL}$, can be obtained via Kramers-Kronig transformation[43,44]. The dielectric function is related to the complex index of refraction $\widetilde{n}$ as follows:

$$\widetilde{\varepsilon}(E_p) = \varepsilon_\infty + \widetilde{\varepsilon}_{TL}(E_p) = [n(E_p) + ik(E_p)]^2 \equiv \widetilde{n}^2(E_p). \tag{3}$$

Here $n(E_p)$ and $k(E_p)$ are the real index of refraction and the absorption coefficient, respectively.

Model parameters were thickness d, TL parameters A_{TL}, B_{TL}, $E_{0,TL}$, and $E_{g,TL}$, and high-frequency dielectric constant ε_∞.

To minimize unwanted parameter correlations, a multi-sample analysis (MSA) was performed, i.e. multiple datasets from a set of samples were analyzed simultaneously. Some parameters were assumed to be the same for all samples (coupled parameters). The other

parameters were varied independently for each sample (uncoupled parameters). In total, the datasets of 113 samples were analyzed using one MSA.

The impact of each model parameter was evaluated with it being uncoupled. The parameters, which made the most impact on the fit quality and showed systematically reasonable variations, were chosen to fit independently. In the end, the uncoupled parameters were the thickness d and the TL parameter A_{TL}, while all other parameters were coupled.

Grazing incidence X-Ray diffraction (GI-XRD, referred as XRD in text) and X-ray reflectivity (XRR) measurements were performed using Cu radiation source at 40 kV and 40 mA in a parallel beam geometry by a Rigaku Ultima IV diffractometer (Tokyo, Japan). Grazing incidence X-ray diffraction measurements are performed at 1° incidence angle, from 10° to 90° with a step size of 0.02° and a scan speed of 1°/min. The XRR patterns were obtained with a step size of 0.002° and a scan speed of 0.25°/min. XRR data analysis was conducted with the Globalfit software[50].

The surface topography was measured by atomic force microscopy (AFM) with a large sample scanning force microscope Bruker Dimension ICON. The device was operated in Tapping Mode$^{\mathrm{TM}}$ and in xy-closed loop configuration. An area of (2×2) $\mu\mathrm{m}^2$ was scanned with a resolution of 1024×1024 pixels. The root mean square (RMS) roughness was calculated from the images.

The composition of selected gallium oxide films was determined by Rutherford backscattering spectrometry (RBS) measurements using singly charged He ions with an energy of 1.9 MeV. The RBS spectra were analyzed with regard to film composition and thickness using XRUMP[51].

Time-of-flight secondary ion mass spectrometry (ToF-SIMS; system "TOF.SIMS 5" by IONTOF) was used for depth profiling of the thin film sample composition. The analysis was done by a 15 keV Ga^+ ion beam, while the analysis scan field of (50×50) $\mu\mathrm{m}^2$ is centered within the (300×300) $\mu\mathrm{m}^2$ sputter crater. Film composition including trace element profiling is performed in positive mode with a mass resolution of 8500. For sputtering a 1 keV Ar^+ ion beam is used. The depth calibrations are provided by white light interferometry analysis of the sputter crater depths. For quantitative evaluation of the gallium oxide film composition, the relative sensitivity factor for oxygen is determined from RBS measurements.

III. RESULTS

A. Film thickness and growth rates

Measured values of maximum film thicknesses $d_{\max}$ per parameter set are given in Table I. To compare the results of different sample sets, the maximum thickness in a set was targeted to be similar by adjusting the deposition times. Hence, it is more practical to compare the growth rates between the sets of samples, which are obtained by dividing the thickness by deposition time.

Figure 2 shows the polar plots of growth rates as a function of the polar emission angle β. All angular distributions have an over-cosine, forward-tilted shape with a maximum at angles between $\beta = 10°$ and $\beta = 40°$. Similar tilted angular distributions were observed previously for other materials[33,40]. An over-cosine shape and tilt of the distribution are attributed to so-called "anisotropy effects"[52,53], caused by an incomplete evolution of the collision cascades inside the target when the primary ions hit the target at a non-normal incidence or with low energy. In these cases, energy is deposited closer to the surface and the collision cascades become shorter because the recoil particles may leave the target after only a few collisions.

The growth rate increases with increasing ion incidence angle α [Figure 2(a)] and increasing ion energy E_{ion} [Figure 2(b)], showing the impact of those parameters on the sputtering yield Y[52]. The growth rate as the function of the O_2 partial pressure does not significantly change in case of an O_2^+ ion beam [Figure 2(c)] and decreases with increasing pressure in case of Ar^+ bombardment [Figure 2(d)]. The latter is related to the oxidation of the target. As shown earlier[54,55], the near-surface region of an oxygen-containing target becomes oxygen-deficient due to preferential sputtering when noble gas ions are used as primary species and no background oxygen is supplied. If there is a supply of background O_2, the surface is reoxidized. The degree of oxidization increases with the background pressure and the sputter yield from a more-oxidized target is usually lower than from a less-oxidized[56], hence the growth rate of the film decreases.
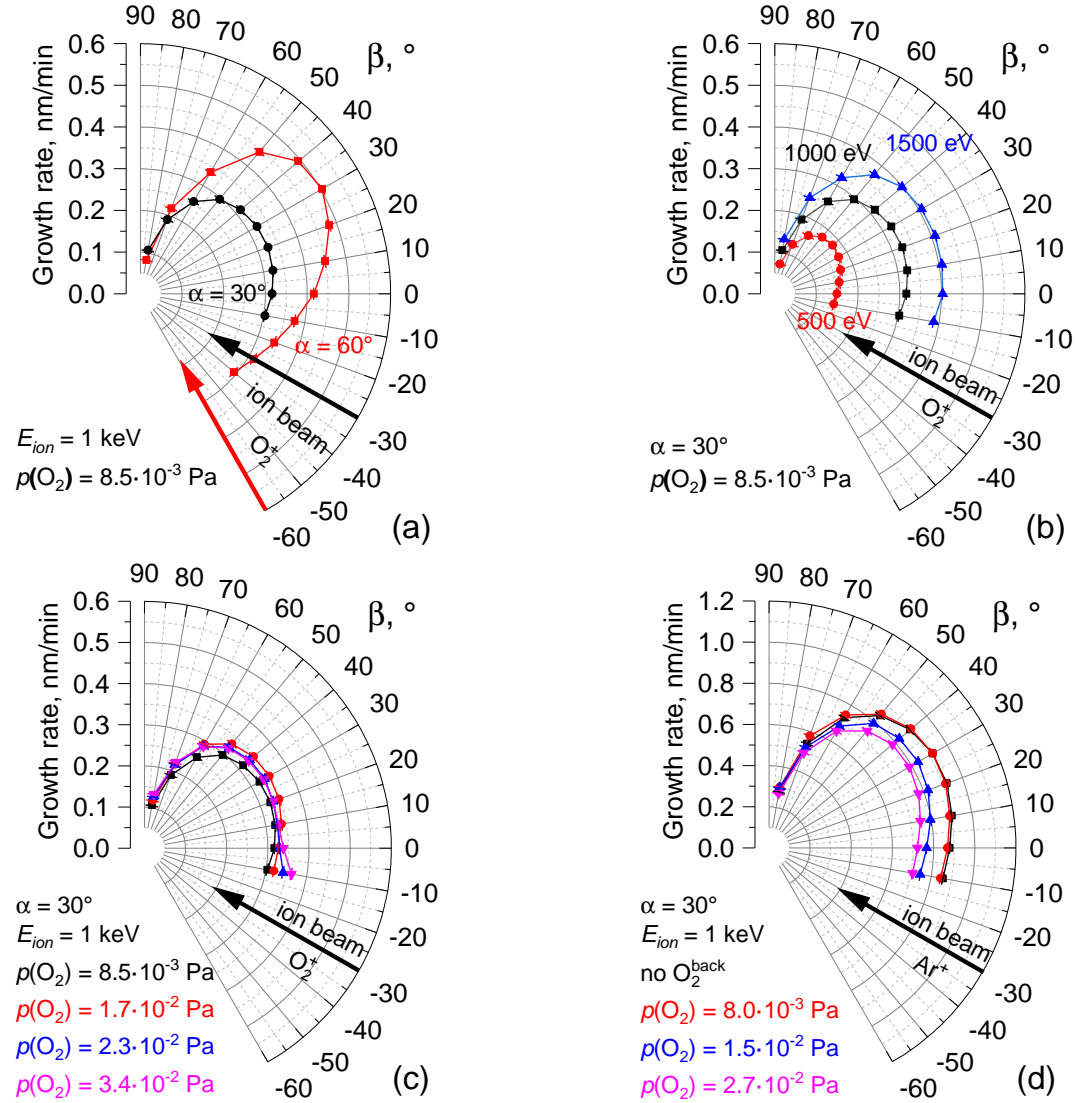
FIG. 2. Growth rates of gallium oxide thin films grown by IBSD using O_2^+ ion beam (a,b,c) or Ar^+ ion beam (d) as functions of polar emission angle β in dependence on different process parameters: ion incidence angle (a), incident ion energy (b), and O_2 background pressure (c,d). The scale in panel (d) is twice the scale in panels (a,b,c).

B. Crystallinity and roughness

XRD patterns of selected gallium oxide films, measured in grazing incidence configuration, are presented in Figure 3. There is no sign of the crystalline phases in the diffraction patterns and the films can be described as amorphous. There has been no significant change observed in diffraction patterns regarding different sets of deposition parameters. However, it is possible to recognize a pronounced hump in the patterns (for example, O_2^+ ion beam case in
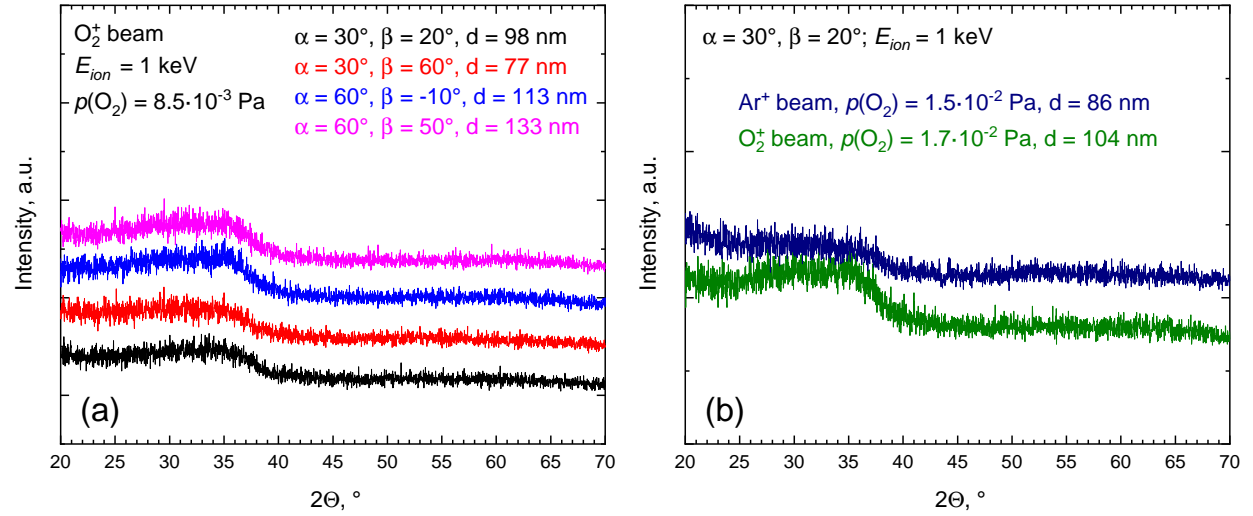
FIG. 3. GI-XRD patterns of selected gallium oxide thin films grown by IBSD on Si substrates at room temperature using O_2^+ ion beam (a,b) or Ar^+ ion beam (b) for different combinations of ion incidence and polar emission angles (a), primary ion beam species in presence of background oxygen (b).

Figure 3b). Although it is not trivial to distinguish between a nanocrystalline and amorphous structure in XRD measurements, the position of the amorphous hump coincides with the two main peaks of the crystalline β-Ga_2O_3 phase[34], which means that some crystallization may take place in the amorphous matrix. The small differences in the pattern shapes can be influenced by thickness differences and the impact of the secondary Ar particles in case of Ar^+ ion beam and are therefore inconclusive.

As determined by AFM and confirmed by XRR measurements, the roughness of the samples yields RMS values below 1 nm without clear correlations to variations of process parameters.

C.   Mass density

Figure 4 summarizes the mass density of selected gallium oxide samples, obtained from XRR measurements. The data show no clear systematic correlations with ion energy, incidence angle, ion species, or background oxygen pressure. Nevertheless, a slight decrease in the mass density with increasing emission angle can be noticed. It was shown earlier, that increasing emission angle leads to the increase in the average energy of film-forming particles[35]. There are competing processes, in particular, film densification and defect for-
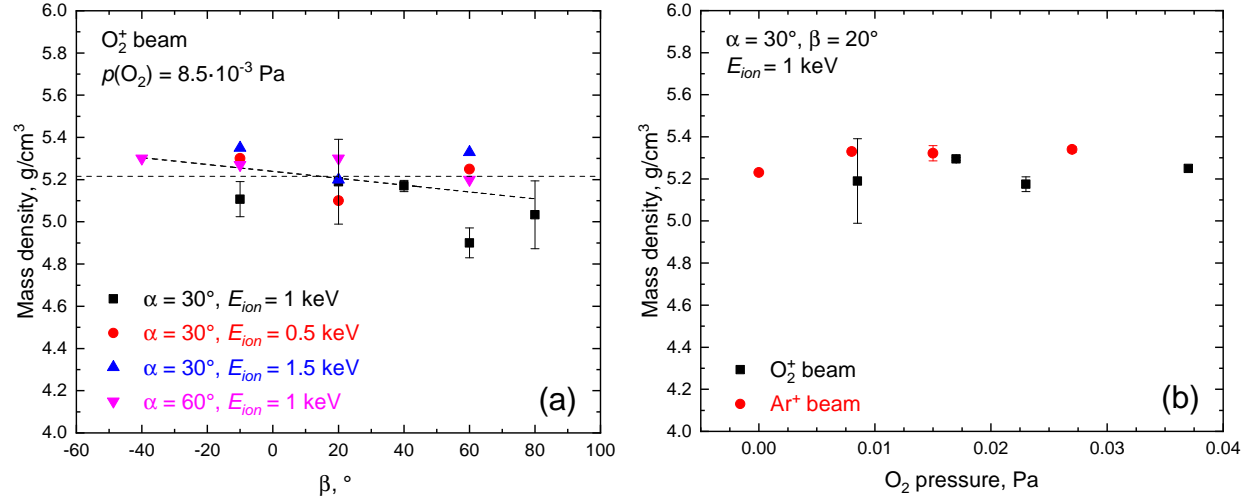
FIG. 4. Mass density measured by XRR for selected gallium oxide thin films grown by IBSD using O_2^+ ion beam (a,b) or Ar^+ ion beam (b) with different process parameter sets as a function of polar emission angle β for different incident ion energies or angles of incidence (a) and O_2 background pressure for different primary ion species (b).

mation. With the increase of particle energy, first, the film density increases due to the enhancement of surface and bulk mobility. If the energy exceeds a certain threshold value, defect formation becomes dominating. This leads to a decrease of mass density[40,57–59].

The averaging over all measured data gives a mean mass density value of (5.2 ± 0.2) g/cm^3. Areal atomic density data from RBS measurements combined with film thickness data yields similar mass density values about 5% lower. The measured density values are similar to those previously reported for amorphous gallium oxide thin films[31,32,60,61], generally not exceeding 90% of the bulk density of β-Ga$_2$O$_3$ (5.95 g/cm^3,[62]).

D. Composition

RBS measurements of selected thin films showed oxygen concentrations of about 59 at.% - 63 at.%. In the films, deposited by sputtering with Ar^+ ion beam, small traces (0.5 at.% - 0.6 at.%) of implanted Ar are observed. Also, the films contained traces of W (< 1 at.%) from the hot filament of the ion beam neutralizer. Figure 5 summarizes the data on the O/Ga ratios versus scattering angle γ (a), energy of incident ions (b), and background O_2 pressure for different primary ion species (c). The O/Ga ratio tends to slightly decrease with increasing emission angle β or increasing ion energy E_{ion}, from O/Ga ratio ≈ 1.7 towards the
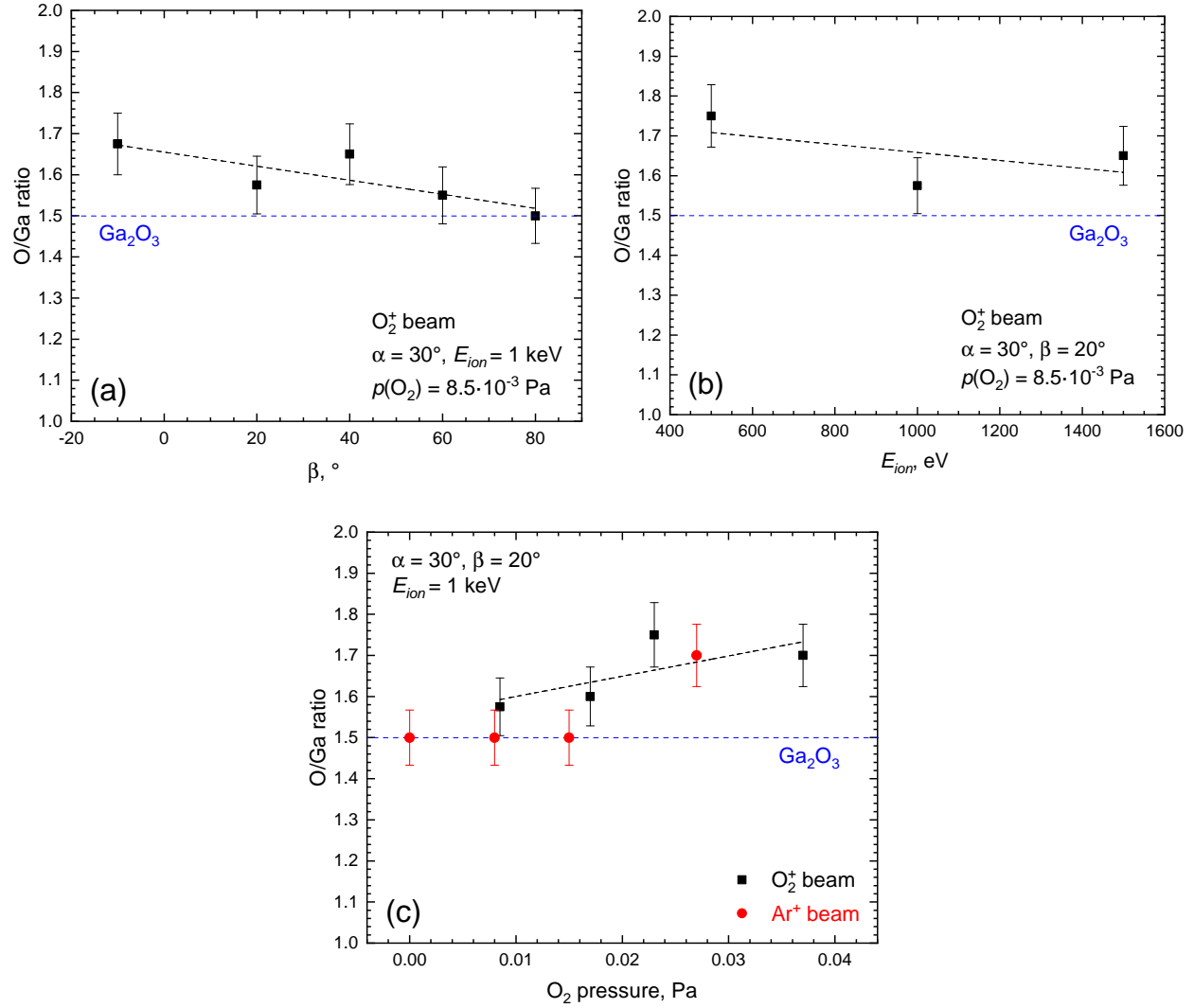
FIG. 5. O/Ga atomic fraction ratios measured by RBS for selected gallium oxide thin films grown by IBSD using O_2^+ ion beam (a,b,c) or Ar^+ ion beam (c) with different process parameter sets as functions of polar emission angle β (a), incident ion energy (b), or O_2 background pressure for different primary ion species (c).

stoichiometric O/Ga ratio ≈ 1.5 for Ga_2O_3. This improvement of stoichiometry correlates with the increase of the average energy of film-forming ions at higher β or higher E_{ion}[35]. Faster secondary particles provide more intrinsic heating to the growing film, promoting the rearrangement of atoms in the lattice. The opposite effect is observed with the increasing background O_2 pressure: O/Ga ratio increases.

The overstoichiometric O/Ga ratio of about 1.6 was also previously reported for films grown by magnetron sputtering at room temperature[28]. With an increase of the substrate
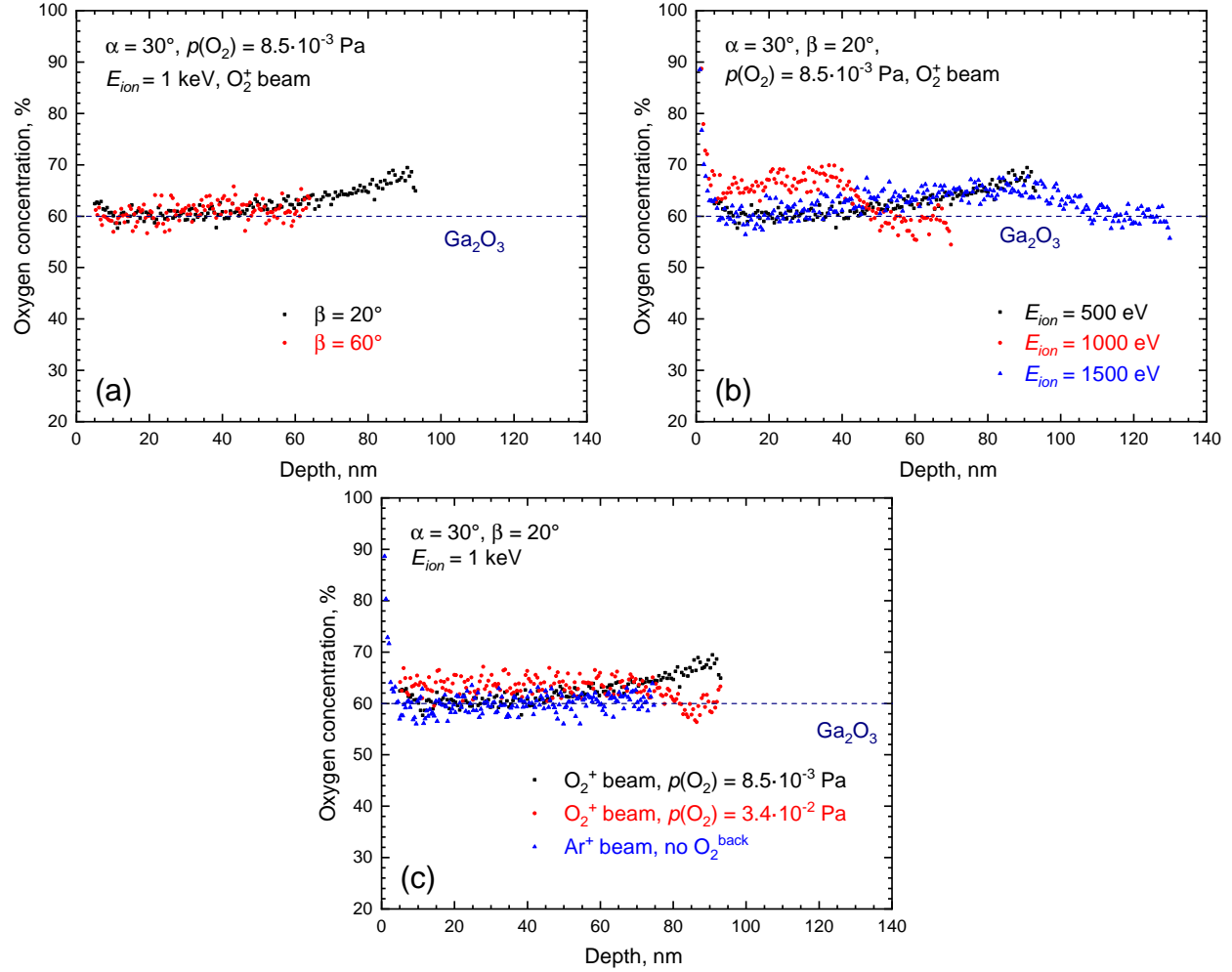
FIG. 6. Depth profile of oxygen concentration measured by SIMS for selected gallium oxide thin films grown by IBSD using O_2^+ ion beam (a,b,c) or Ar^+ ion beam (c) with different process parameter sets: variation of the polar emission angle β (a), incident ion energy (b), or O_2 background pressure and primary ion species (c).

temperature, stoichiometry had improved. Present observations are in agreement with that change in stoichiometry, with the difference that the current effect is due to the impact of film-forming energetic particles instead of substrate heating.

Figure 6 shows SIMS depth profiles for the relative oxygen concentration for selected samples. The oxygen concentration is determined from the intensity ratio of the $^{71}GaO^+$ signal to the $^{71}Ga_2^+$ signal. A relative sensitivity factor of 320 ± 15 is applied as obtained from the RBS results. There are small changes of the oxygen concentration with depth, but no systematic correlations to process parameters are observed.

13

E. Optical properties

The best-fit MDF parameters from the multisample ellipsometric data analysis are listed in Table II. Figure 7 shows the uncoupled Tauc-Lorentz (TL) parameter A_{TL} versus emission angle β in dependence on different process parameters. Overall, a decrease of A_{TL} with increasing β is observed for all sets involving primary O_2^+ ions [Figures 7(a,b,c)]. Also, the A_{TL} are slightly increasing with increasing angle of incidence α [Figure 7(a)] or increasing background O_2 pressure [Figure 7(c)]. A_{TL} does not show a clear dependence on the ion energy [Figure 7(b)], except for the slight change in the shape of angular distribution. Parameter sets with primary Ar^+ ions [Figure 7(d)] show somewhat different angular distributions. When background oxygen is present, A_{TL} monotonously decreases, and the decrease is more prominent than with primary oxygen ions. If no background oxygen is present, the angular distribution has a distinct shape (black line): at first, the value increases and then drops after $\beta = 40°$.

These effects can be associated with the impact of film-forming particles through correlation with index of refraction and mass density. Figure 8 shows spectra of the index of refraction n for selected samples. In Figure 9 the index of refraction n at a wavelength of $\lambda = 633$ nm is plotted as a function of the mass density. It shows that the index of refraction and mass density are correlated, which was also previously observed for IBSD of TiO_2 and SiO_2[33]. The index of refraction and A_{TL} are generally decreasing with increasing energy of film-forming species, and, therefore, kinetic impact on the growing film. The general change in shapes of $A_{TL}(\beta)$ distributions in the case of primary Ar^+ ions may be partially explained by the presence of fast Ar particles, scattered from the target[35], which bring additional energy to the surface and, hence, the faster decrease at higher β. When no background oxygen is supplied to the system (Figure 8(d), black data points), the $A_{TL}(\beta)$ distribution appears noticeably different even to other cases involving Ar^+ ions. Although there is no full understanding behind this difference in shape, the sputtering with and without a surrounding oxygen atmosphere is distinctly different. If no additional oxygen is present, the target surface faces an oxygen deficiency due to preferential sputtering. Therefore, the amount of sputtered oxygen particles is limited to those already present in the target. By adding oxygen background gas, the target surface gets reoxidized and more oxygen can be sputtered. Previous studies of the properties of secondary particles confirmed this[35]. It was shown that

TABLE II. Best-fit Tauc-Lorentz model parameters of the multisample ellipsometric data analysis of gallium oxide thin films grown by IBSD. Numbers in parenthesis represent the 90% confidence limits.

Parameter	Value
Number of samples	113
ε_∞	1.83 ($< \pm 0.01$)
A_{TL}[a]	124-160 (± 0.6)
$E_{\mathrm{g,TL}}$ (eV)	4.25 ($< \pm 0.01$)
$E_{\mathrm{0,TL}}$ (eV)	5.62 ($< \pm 0.01$)
B_{TL} (eV)	5.40 (± 0.01)

[a] Parameter is varied independently for each sample (uncoupled).

the energy distributions of secondary oxygen ions (atomic and molecular) gain considerable intensity upon switching on the oxygen background gas, while the further increase of oxygen background pressure almost does not affect the energy distributions. The energy distributions of sputtered Ga ions and scattered Ar ions show only small changes. Furthermore, an understoichiometric composition can be expected in this case, which may be related to the uncertainty in RBS data [Figure 5c]. This understoichiometry would affect the electronic structure of the material and, hence, the dielectric function and the Tauc-Lorentz parameters. However, it should be studied further to gain a deeper understanding.

The values of the optical band gap E_{g} and index of refraction n at a wavelength of $\lambda = 633$ nm, obtained for amorphous gallium oxide thin films from ellipsometric analysis in this work and in literature[23,25,26,29], are presented in Table III. The index of refraction n ($\lambda = 633$ nm) yields same values around 1.8-1.9. The ellipsometric study of the epitaxial $\beta-\mathrm{Ga_2O_3}$ films and single crystals reported values of 1.9-2.0[47].

The optical band gap E_{g} in the present work is a coupled parameter in the multisample analysis. The resulting value of 4.25 eV is slightly lower than in Refs.[25,26], which reported 4.51 eV and (4.63 ± 0.05) eV, respectively. The optical band gap energies of epitaxial $\beta-\mathrm{Ga_2O_3}$ films were reported to be in the range of ($4.4 - 5$) eV, Ref.[47].

TABLE III. Band gap energy E_g and index of refraction n of amorphous gallium oxide thin films, obtained from the ellipsometric analysis. Data were taken from this work and Refs.[23,25,26,29].

	This work	Ref.[25]	Ref.[26]	Ref.[29]	Ref.[23]
Deposition technique	IBSD	ALD	PEALD	RF-MS	RF-MS, EBE
MDF model	Tauc-Lorentz	Tauc-Lorentz	Tauc-Lorentz	Cauchy	Cauchy
E_g (eV)	4.25 ($< \pm0.01$)	4.51	4.63 (±0.05)	-	-
n ($\lambda \approx 633$ nm)	1.83 - 1.88	1.91	1.85 (±0.01)	1.8[a]	1.89

[a] Value taken for the samples grown at room temperature, Figure 8 from Ref.[29]

IV. CONCLUSIONS

Gallium oxide thin films were grown by IBSD from a ceramic Ga_2O_3 target with systematically varied process parameters, such as sputtering geometry (ion incidence angle α and polar emission angle β), incident ion energy, ion species, and background oxygen pressure. The films were grown on Si substrates at room temperature to focus on the influence of film-forming species on the film properties, such as kinetic impact and intrinsic heating. The following film properties were investigated: film thicknesses, growth rates, crystallinity, surface roughness, mass density, elemental composition and its depth profiles, and optical properties.

All deposited films were smooth (RMS roughness < 1 nm) and amorphous regardless of the process parameters. The angular distributions of the growth rates have over-cosine shapes with maximum values between $\beta = 10°$ and $\beta = 40°$. Higher incidence angle α and higher energy of primary ions increase the growth rate. The increase of the background oxygen pressure has no significant effect on the growth rate in the case of the O_2^+ ion beam, but leads to its reduction in the case of the Ar^+ ion beam due to the oxidation of the target. Sputtering with Ar^+ ions has 2-3 times higher sputter yield than with O_2^+ ions, which is expected but brings up another topic: the elemental composition of the film. The use of Ar^+ ions leads to implantation of fast scattered Ar particles into the film, yielding a relative amount of 0.5 at.% - 0.6 at.%. Whether this can be tolerated depends on the particular application for the deposited gallium oxide films. Additionally, traces of W (< 1 at.%) were found, which originate from the hot-filament beam neutralizer. The use of a
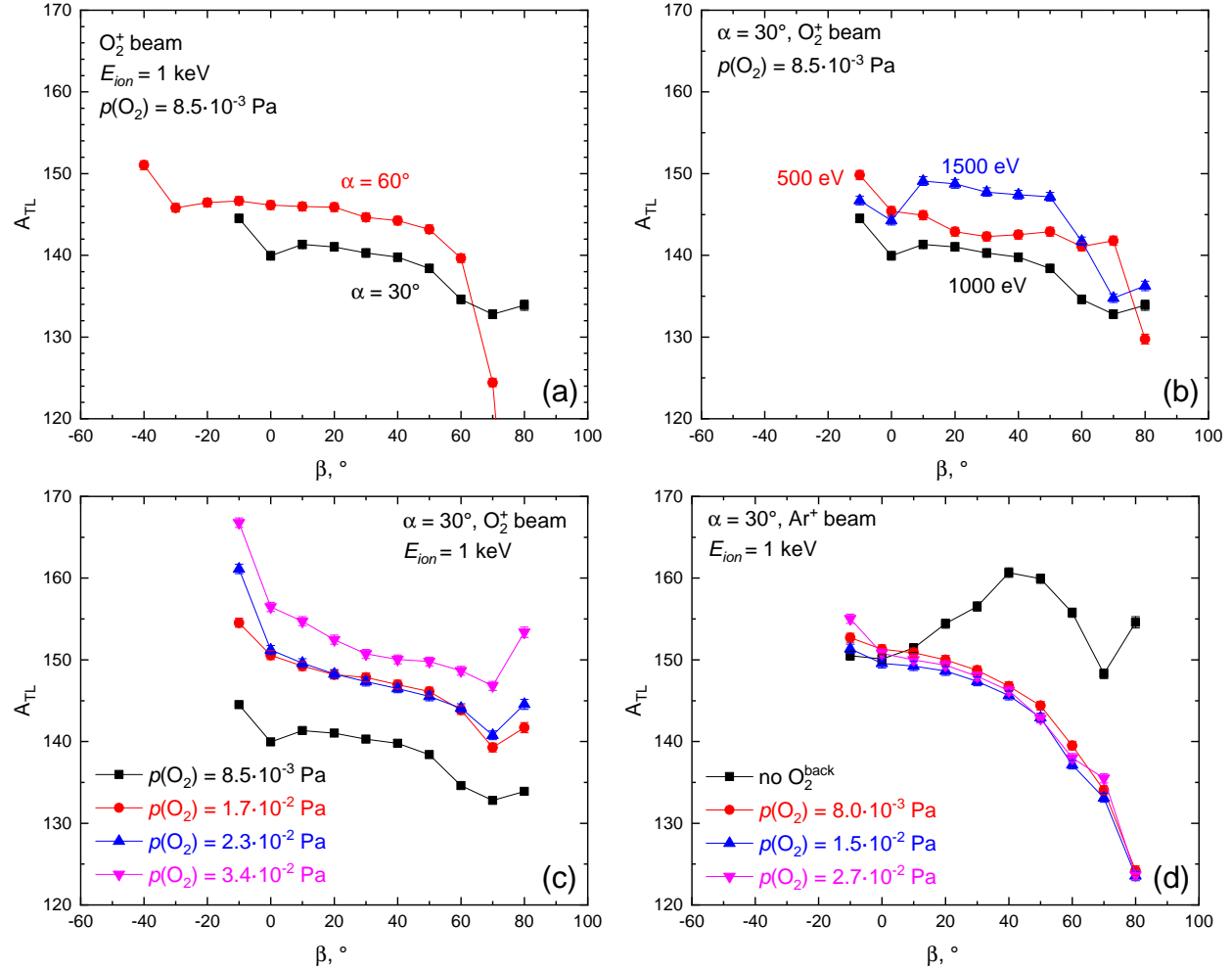
FIG. 7. Best-fit model parameter A_{TL} as a function of emission angle β of the multisample analysis of the ellipsometric data of gallium oxide thin films grown by reactive IBSD using O_2^+ ion beam (a,b,c) or Ar^+ ion beam (d). Data are shown in dependence on ion incidence angle α (a), ion energy E_{ion} (b), O_2 background pressure (c,d).

shield between the primary ion beam and the substrate holder, or an RF plasma bridge neutralizer[63] can be used to avoid the contamination. The analysis of the O/Ga ratio shows that the stoichiometry close to the desired value of 1.5 is achieved at higher ion energies and polar emission angles, and lower background oxygen pressures. This effect is correlated with the increase of the average energy of film-forming species. Next, the depth profiles of the oxygen concentration show no systematic dependencies on the process parameters. Finally, the mass density and the optical properties, such as the index of refraction n, show a noticeable correlation and confirm the expected dependency on the kinetic impact of the film-forming ions. However, unlike the O/Ga ratio, they tend to decrease with increasing β,
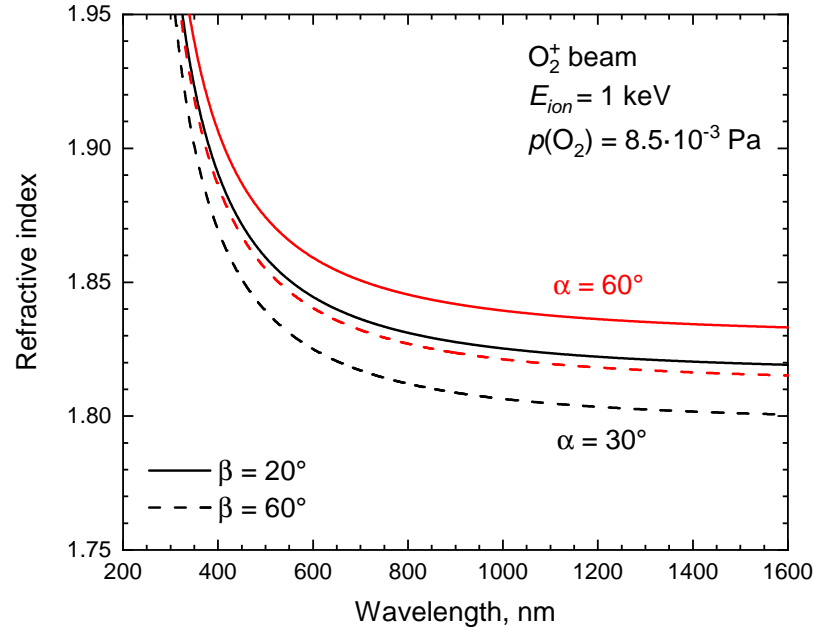
FIG. 8. Index of refraction n of selected gallium oxide thin films grown by IBSD using O_2^+ ion beam in different sputtering geometries as a function of wavelength.
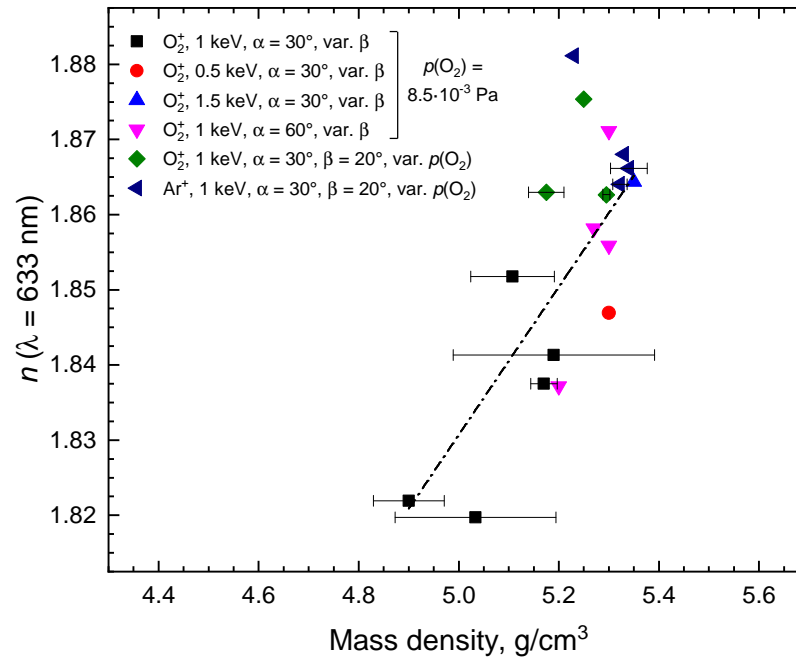

FIG. 9. Index of refraction n at $\lambda = 633$ nm as a function of mass density of gallium oxide thin films grown by IBSD with different parameter sets. The dash-dotted line represents a linear fit to the combined set of scattered data.

which can be related to the formation of defects due to excessively high energies of secondary

particles that impact the growing film.

To sum up the analysis: The energetic impact of film-forming species is not sufficient for the growth of crystalline gallium oxide films at room temperature, and substrate heating is still necessary. However, the effects of energetic impact on the growth rate, film stoichiometry, mass density, and optical properties are present. By taking the values of these parameters reported for epitaxial β-Ga_2O_3 films by others as reference, the following IBSD configuration can be chosen within the parameter ranges of the present work: O_2^+ ions as primary species, $E_{ion} = 1000$ eV or higher, $\alpha = 60°$, $10° < \beta < 40°$, and O_2 background pressure $< 10^{-2}$ Pa. In these conditions, the O/Ga ratio tends to be closer to 1.5, and mass density, optical quality and the growth rate tend to be higher. The current study can help to tailor the IBSD process for the growth of Ga_2O_3 films of higher quality in future experiments (e.g., involving substrate heating and other substrate materials, such as sapphire or β-Ga_2O_3) by utilizing moderately energetic film-forming species.

ACKNOWLEDGMENTS

AUTHOR DECLARATIONS

Conflict of Interest

The authors have no conflicts to disclose.

DATA AVAILABILITY STATEMENT

The data that support the findings of this study are available from the corresponding author upon reasonable request.

REFERENCES

[1]S. J. Pearton, J. Yang, P. H. Cary, F. Ren, J. Kim, M. J. Tadjer, and M. A. Mastro, "A review of Ga_2O_3 materials, processing, and devices," Applied Physics Reviews **5**, 011301 (2018).

[2]S. J. Pearton, F. Ren, and M. A. Mastro, *Gallium oxide: Technology, devices and applications*, edited by G. Korotchenkov (Elsevier, 2019).

[3]K. Matsuzaki, H. Hiramatsu, K. Nomura, H. Yanagi, T. Kamiya, M. Hirano, and H. Hosono, "Growth, structure and carrier transport properties of Ga_2O_3 epitaxial film examined for transparent field-effect transistor," Thin Solid Films **496**, 37 (2006).

[4]M. Higashiwaki, K. Sasaki, A. Kuramata, T. Masui, and S. Yamakoshi, "Gallium oxide (Ga_2O_3) metal-semiconductor field-effect transistors on single-crystal β-Ga_2O_3 (010) substrates," Applied Physics Letters **100**, 013504 (2012).

[5]S. J. Pearton, F. Ren, M. Tadjer, and J. Kim, "Perspective: Ga_2O_3 for ultra-high power rectifiers and MOSFETS," Journal of Applied Physics **124**, 220901 (2018).

[6]T. Minami, Y. Nishi, and T. Miyata, "High-Efficiency Cu_2O-Based Heterojunction Solar Cells Fabricated Using a Ga_2O_3 Thin Film as N-Type Layer," Applied Physics Express **6**, 044101 (2013).

[7]T. Koida, Y. Kamikawa-Shimizu, A. Yamada, H. Shibata, and S. Niki, "Cu(In,Ga)Se$_2$ Solar Cells With Amorphous Oxide Semiconducting Buffer Layers," IEEE Journal of Photovoltaics **5**, 956 (2015).

[8]M. D. Heinemann, J. Berry, G. Teeter, T. Unold, and D. Ginley, "Oxygen deficiency and Sn doping of amorphous Ga_2O_3," Applied Physics Letters **108**, 022107 (2016).

[9]T. G. Allen, Y. Y. Wan, and A. Cuevas, "Silicon Surface Passivation by Gallium Oxide Capped with Silicon Nitride," IEEE Journal of Photovoltaics **6**, 900 (2016).

[10]G. Wagner, M. Baldini, D. Gogova, M. Schmidbauer, R. Schewski, M. Albrecht, Z. Galazka, D. Klimm, and R. Fornari, "Homoepitaxial growth of β-Ga_2O_3 layers by metal-organic vapor phase epitaxy," physica status solidi (a) **211**, 27 (2014).

[11]D. Gogova, G. Wagner, M. Baldini, M. Schmidbauer, K. Irmscher, R. Schewski, Z. Galazka, M. Albrecht, and R. Fornari, "Structural properties of Si-doped β-Ga_2O_3 layers grown by MOVPE," Journal of Crystal Growth **401**, 665 (2014).

[12]T. S. Chou, P. Seyidov, S. Bin Anooz, R. Grüneberg, T. T. V. Tran, K. Irmscher, M. Albrecht, Z. Galazka, J. Schwarzkopf, and A. Popp, "Fast homoepitaxial growth of (100) β-Ga$_2$O$_3$ thin films via MOVPE," AIP Advances **11**, 115323 (2021).

[13]E. G. Víllora, K. Shimamura, K. Kitamura, and K. Aoki, "RF-plasma-assisted molecular-beam epitaxy of β-Ga$_2$O$_3$," Applied Physics Letters **88**, 031105 (2006).

[14]T. Oshima, N. Arai, N. Suzuki, S. Ohira, and S. Fujita, "Surface morphology of homoepitaxial β-Ga$_2$O$_3$ thin films grown by molecular beam epitaxy," Thin Solid Films **516**, 5768 (2008).

[15]K. Sasaki, M. Higashiwaki, A. Kuramata, T. Masui, and S. Yamakoshi, "Growth temperature dependences of structural and electrical properties of Ga$_2$O$_3$ epitaxial films grown on β-Ga$_2$O$_3$ (010) substrates by molecular beam epitaxy," Journal of Crystal Growth **392**, 30 (2014).

[16]P. Vogt and O. Bierwagen, "The competing oxide and sub-oxide formation in metal-oxide molecular beam epitaxy," Applied Physics Letters **106**, 081910 (2015).

[17]P. Vogt and O. Bierwagen, "Reaction kinetics and growth window for plasma-assisted molecular beam epitaxy of Ga$_2$O$_3$: Incorporation of Ga vs. Ga$_2$O desorption," Applied Physics Letters **108**, 072101 (2016).

[18]Y. Oshima, E. Ahmadi, S. Kaun, F. Wu, and J. S. Speck, "Growth and etching characteristics of (001) β-Ga$_2$O$_3$ by plasma-assisted molecular beam epitaxy," Semiconductor Science and Technology **33**, 015013 (2017).

[19]S. J. Hao, M. Hetzl, F. Schuster, K. Danielewicz, A. Bergmaier, G. Dollinger, Q. L. Sai, C. T. Xia, T. Hoffmann, M. Wiesinger, S. Matich, W. Aigner, and M. Stutzmann, "Growth and characterization of β-Ga$_2$O$_3$ thin films on different substrates," Journal of Applied Physics **125**, 105701 (2019).

[20]S. Müller, H. Von Wenckstern, D. Splith, F. Schmidt, and M. Grundmann, "Control of the conductivity of Si-doped β-Ga$_2$O$_3$ thin films via growth temperature and pressure," physica status solidi (a) **211**, 34 (2014).

[21]M. Kneiß, A. Hassa, D. Splith, C. Sturm, H. Von Wenckstern, T. Schultz, N. Koch, M. Lorenz, and M. Grundmann, "Tin-assisted heteroepitaxial PLD-growth of κ-Ga$_2$O$_3$ thin films with high crystalline quality," APL Materials **7**, 022516 (2019).

[22]M. Passlack, E. F. Schubert, W. S. Hobson, M. Hong, N. Moriya, S. N. Chu, K. Konstadinidis, J. P. Mannaerts, M. L. Schnoes, and G. J. Zydzik, "Ga$_2$O$_3$ films for electronic and

optoelectronic applications," Journal of Applied Physics **77**, 686 (1995).

[23]M. Rebien, W. Henrion, M. Hong, J. P. Mannaerts, and M. Fleischer, "Optical properties of gallium oxide thin films," Applied Physics Letters **81**, 250 (2002).

[24]E. Kobayashi, M. Boccard, Q. Jeangros, N. Rodkey, D. Vresilovic, A. Hessler-Wyser, M. Döbeli, D. Franta, S. De Wolf, M. Morales-Masis, and C. Ballif, "Amorphous gallium oxide grown by low-temperature PECVD," Journal of Vacuum Science and Technology A **36**, 021518 (2018).

[25]H. Y. Shih, F. C. Chu, A. Das, C. Y. Lee, M. J. Chen, and R. M. Lin, "Atomic Layer Deposition of Gallium Oxide Films as Gate Dielectrics in AlGaN/GaN Metal–Oxide–Semiconductor High-Electron-Mobility Transistors," Nanoscale Research Letters **11**, 235 (2016).

[26]A. Mahmoodinezhad, C. Janowitz, F. Naumann, P. Plate, H. Gargouri, K. Henkel, D. Schmeißer, and J. I. Flege, "Low-temperature growth of gallium oxide thin films by plasma-enhanced atomic layer deposition," Journal of Vacuum Science and Technology A **38**, 022404 (2020).

[27]P. Marie, X. Portier, and J. Cardin, "Growth and characterization of gallium oxide thin films by radiofrequency magnetron sputtering," physica status solidi (a) **205**, 1943 (2008).

[28]S. S. Kumar, E. J. Rubio, M. Noor-A-Alam, G. Martinez, S. Manandhar, V. Shutthanandan, S. Thevuthasan, and C. V. Ramana, "Structure, morphology, and optical properties of amorphous and nanocrystalline gallium oxide thin films," Journal of Physical Chemistry C **117**, 4194 (2013).

[29]C. V. Ramana, E. J. Rubio, C. D. Barraza, A. Miranda Gallardo, S. McPeak, S. Kotru, and J. T. Grant, "Chemical bonding, optical constants, and electrical resistivity of sputter-deposited gallium oxide thin films," Journal of Applied Physics **115**, 043508 (2014).

[30]N. Makeswaran, A. K. Battu, E. Deemer, and C. V. Ramana, "Crystal Growth and Structure-Property Optimization of Thermally Annealed Nanocrystalline Ga_2O_3 Films," Crystal Growth and Design **20**, 2893 (2020).

[31]Y. Pei, L. Liang, X. L. Wang, K. Wang, H. B. Zhang, Z. D. Wu, H. J. Wu, H. Zhang, J. Gao, and H. Cao, "Substrate-bias-aided preparation and properties of amorphous gallium oxide films and their deep-ultraviolet photodetectors," Ceramics International **47**, 32138 (2021).

[32]A. K. Singh, M. Gupta, V. Sathe, and Y. S. Katharria, "Effect of annealing temperature on β-Ga_2O_3 thin films deposited by RF sputtering method," Superlattices and Microstruc-

tures **156**, 106976 (2021).

[33]C. Bundesmann and H. Neumann, "Tutorial: The systematics of ion beam sputtering for deposition of thin films with tailored properties," Journal of Applied Physics **124**, 231102 (2018).

[34]M. Becker, S. L. Benz, L. Chen, A. Polity, P. J. Klar, and S. Chatterjee, "Controlled thin-film deposition of α or β-Ga_2O_3 by ion-beam sputtering," Journal of Vacuum Science and Technology A **38**, 063412 (2020).

[35]D. Kalanov, A. Anders, and C. Bundesmann, "Properties of secondary ions in ion beam sputtering of Ga_2O_3," Journal of Vacuum Science and Technology A **39**, 053409 (2021).

[36]M. Zeuner, F. Scholze, B. Dathe, and H. Neumann, "Optimisation and characterisation of a TCP type RF broad beam ion source," Surface and Coatings Technology **142-144**, 39 (2001).

[37]R. Feder, F. Frost, H. Neumann, C. Bundesmann, and B. Rauschenbach, "Systematic investigations of low energy Ar ion beam sputtering of Si and Ag," Nuclear Instruments and Methods in Physics Research B **317**, 137 (2013).

[38]T. Lautenschläger, *Systematic investigation of the ion beam sputter deposition of TiO_2*, Ph.D. thesis, University of Leipzig (2018).

[39]D. Kalanov, A. Anders, and C. Bundesmann, "Ion beam sputtering of silicon: Energy distributions of sputtered and scattered ions," Journal of Vacuum Science and Technology A **37**, 051507 (2019).

[40]C. Bundesmann, J. Bauer, A. Finzel, J. W. Gerlach, W. Knolle, A. Hellmich, and R. Synowicki, "Properties of indium tin oxide thin films grown by Ar ion beam sputter deposition," Journal of Vacuum Science and Technology A **39**, 033406 (2021).

[41]H. R. Kaufman, "Technology of ion beam sources used in sputtering," Journal of Vacuum Science and Technology **15**, 272 (1978).

[42]C. M. Herzinger, B. Johs, W. A. McGahan, J. A. Woollam, and W. Paulson, "Ellipsometric determination of optical constants for silicon and thermally grown silicon dioxide via a multi-sample, multi-wavelength, multi-angle investigation," Journal of Applied Physics **83**, 3323 (1998).

[43]G. E. Jellison and F. A. Modine, "Parameterization of the optical functions of amorphous materials in the interband region," Applied Physics Letters **69**, 371 (1996).

[44]G. E. Jellison and F. A. Modine, "Erratum: Parameterization of the optical functions of amorphous materials in the interband region [Appl. Phys. Lett. (1996) 69 (371) (10.1063/1.118064))," Applied Physics Letters **69**, 2137 (1996).

[45]H. Fujiwara, *Spectroscopic ellipsometry: Principles and applications* (John Wiley and Sons, 2007).

[46]T. G. Allen and A. Cuevas, "Electronic passivation of silicon surfaces by thin films of atomic layer deposited gallium oxide," Applied Physics Letters **105**, 031601 (2014).

[47]T. Onuma, S. Saito, K. Sasaki, T. Masui, T. Yamaguchi, T. Honda, A. Kuramata, and M. Higashiwaki, "Spectroscopic ellipsometry studies on β-Ga_2O_3 films and single crystal," Japanese Journal of Applied Physics **55**, 1202B2 (2016).

[48]R. Schmidt-Grund, C. Kranert, T. Böntgen, H. Von Wenckstern, H. Krauß, and M. Grundmann, "Dielectric function in the NIR-VUV spectral range of $(In_xGa_{1-x})_2O_3$ thin films," Journal of Applied Physics **116**, 053510 (2014).

[49]R. Schmidt-Grund, C. Kranert, H. Von Wenckstern, V. Zviagin, M. Lorenz, and M. Grundmann, "Dielectric function in the spectral range (0.5-8.5) eV of an $(Al_xGa_{1-x})_2O_3$ thin film with continuous composition spread," Journal of Applied Physics **117**, 165307 (2015).

[50]M. Yasaka, "X-ray thin-film measurement techniques," The Rigaku Journal **26**, 2 (2010).

[51]L. R. Doolittle, "Algorithms for the rapid simulation of Rutherford backscattering spectra," Nuclear Instruments and Methods in Physics Research B **9**, 344 (1985).

[52]R. Behrisch and W. Eckstein, *Sputtering by particle bombardment* (Springer, Berlin Heidelberg, 2007).

[53]T. Lautenschläger, R. Feder, H. Neumann, C. Rice, M. Schubert, and C. Bundesmann, "Ion beam sputtering of Ti: Influence of process parameters on angular and energy distribution of sputtered and backscattered particles," Nuclear Instruments and Methods in Physics Research B **385**, 30 (2016).

[54]H. Gnaser, "Processes in low-energy ion-surface collisions: Preferential sputtering, defect and adatom formation," Applied Surface Science **100-101**, 316 (1996).

[55]H. Gnaser, *Low-energy ion irradiation of solid surfaces*, Vol. 146 (Springer, Berlin Heidelberg, 1999).

[56]D. R. Baer, M. H. Engelhard, A. S. Lea, P. Nachimuthu, T. C. Droubay, J. Kim, B. Lee, C. Mathews, R. L. Opila, L. V. Saraf, W. F. Stickle, R. M. Wallace, and B. S. Wright, "Comparison of the sputter rates of oxide films relative to the sputter rate of SiO_2," Journal

of Vacuum Science and Technology A **28**, 1060 (2010).

[57] S. Mohan and M. G. Krishna, "A review of ion beam assisted deposition of optical thin films," Vacuum **46**, 645 (1995).

[58] C. Bundesmann, I. M. Eichentopf, S. Mändl, and H. Neumann, "Stress relaxation and optical characterization of TiO_2 and SiO_2 films grown by dual ion beam deposition," Thin Solid Films **516**, 8604 (2008).

[59] L. Pietzonka, T. Lautenschläger, D. Spemann, A. Finzel, J. W. Gerlach, F. Frost, and C. Bundesmann, "Ion beam sputter deposition of TiO_2 films using oxygen ions," European Physical Journal B **91**, 252 (2018).

[60] R. Wakabayashi, T. Oshima, M. Hattori, K. Sasaki, T. Masui, A. Kuramata, S. Yamakoshi, K. Yoshimatsu, and A. Ohtomo, "Oxygen-radical-assisted pulsed-laser deposition of β-Ga_2O_3 and β-$(Al_xGa_{1-x})_2O_3$ films," Journal of Crystal Growth **424**, 77 (2015).

[61] R. O'Donoghue, J. Rechmann, M. Aghaee, D. Rogalla, H. W. Becker, M. Creatore, A. D. Wieck, and A. Devi, "Low temperature growth of gallium oxide thin films via plasma enhanced atomic layer deposition," Dalton Transactions **46**, 16551 (2017).

[62] S. I. Stepanov, V. I. Nikolaev, V. E. Bougrov, and A. E. Romanov, "Gallium oxide: Properties and applications - a review," Reviews on Advanced Materials Science **44**, 63 (2016).

[63] F. Scholze, M. Tartz, and H. Neumann, "Inductive coupled radio frequency plasma bridge neutralizer," Review of Scientific Instruments **79**, 2006 (2008).